

Interplay of screening and superconductivity in low-dimensional materials

G. Schönhoff,^{1,2} M. Rösner,^{1,2} R. Groenewald,³ S. Haas,³ and T. O. Wehling^{1,2}

¹*Institut für Theoretische Physik, Universität Bremen, Otto-Hahn-Allee 1, 28359 Bremen, Germany*

²*Bremen Center for Computational Materials Science,
Universität Bremen, Am Fallturm 1a, 28359 Bremen, Germany*

³*Department of Physics and Astronomy, University of Southern California, Los Angeles, CA 90089-0484, USA*

(Dated: December 3, 2024)

A quantitative description of Coulomb interactions is developed for two-dimensional superconducting materials, enabling us to compare intrinsic with external screening effects, such as those due to substrates. Using the example of a doped monolayer of MoS₂ embedded in a tunable dielectric environment, we demonstrate that the influence of external screening is limited to a length scale, bounded from below by the effective thickness of the quasi two-dimensional material and from above by its intrinsic screening length. As a consequence, it is found that unconventional Coulomb driven superconductivity cannot be induced in MoS₂ by tuning the substrate properties alone. Specifically, our calculations of the retarded Morel-Anderson Coulomb potential μ^* reveal that while the Coulomb interactions renormalized by the reduced layer thickness and the substrate properties can shift the onset of the electron-phonon driven superconducting phase in monolayer MoS₂ at weak doping, they do not significantly affect the critical temperature at optimal doping.

Introduction: Various quasi-two-dimensional (2d) materials are known to exhibit a competition of superconducting (SC), charge density wave, and magnetic phases [1–11], with notably different dependences of the resulting phase diagrams on the number of layers. While in some systems, such as the Fe-based superconductors, the highest transition temperatures T_c are reached in the monolayer limit (e.g. $T_c \sim 100$ K in FeSe on SrTiO₃ substrates [12–15]), several superconducting transition metal dichalcogenides (TMDCs) show exactly the opposite trend of a decreasing T_c when monolayer thickness is approached [6, 7, 9, 16–18]. These observations point towards several competing effects in layered materials, including enhanced quantum fluctuations, singularities in the electronic density of states and response functions, strain, tunable Fermi surface topologies etc., all of which potentially contribute to these trends. In all these cases an important common factor pertains to how the renormalization of Coulomb interactions due to reduced material dimensionality and environmental screening affects the superconducting transition when approaching the monolayer limit.

A representative example for such strongly thickness dependent superconductivity is molybdenum disulfide, MoS₂. This material becomes superconducting upon electron doping, e.g. via intercalation of alkali atoms [1, 2] or by gating [4, 5, 10, 11]. Its temperature-versus-doping phase diagram is characterized by a dome-shape superconducting region, with critical temperatures on the order of a few K at optimal doping, and by a highly anisotropic response to magnetic fields [19, 20]. Recent experiments on field effect doped layered MoS₂ have demonstrated superconductivity down to the monolayer limit, where T_c decreases from ~ 10 K in thicker flakes (> 6 layers) to 2 K for the monolayer [18]. The reason behind this evolution remains elusive. On the theory

side, several scenarios have suggested purely electronic mechanisms giving rise to superconductivity, predicting unconventional [21, 22] and possibly topologically non-trivial types of superconducting order [23]. In contrast, more conventional pathways to superconducting pairing resulting from electron-phonon coupling have also been proposed [24–26]. However, in all of these scenarios it is unclear to which extent the renormalized Coulomb interactions affect superconductivity when approaching the monolayer limit.

In this letter, we develop a quantitative theory of how Coulomb interactions affect the superconducting transition in MoS₂ as a representative example of TMDCs. For purely Coulomb driven superconductivity, a strong renormalization of the interactions e.g. by spin fluctuations [22] would be needed. However, based on *ab initio* calculations we show that a superconducting phase with an order parameter that has opposite signs in different valleys [21] is not favored in MoS₂. We find this to be true rather independently of the dielectric environment of the substrate. For the scenario of phonon mediated SC [24–26], we show that the phonon mediated electron-electron attraction generally overcomes the Coulomb repulsion when a Lifshitz transition takes place and additional Fermi pockets become available. The intrinsic screening of TMDCs at their superconducting transition is shown to be typically so large that it renders external substrate screening rather unimportant despite the atomic scale proximity of the substrate. As a consequence, one finds that the reduced transition temperatures in monolayer MoS₂ as compared to the bulk are not due to a lack of Coulomb screening in the monolayer limit.

Electronic structure and Coulomb interactions: Using density functional theory (DFT) as implemented in Quantum Espresso [27] we obtain the low-energy bands

of monolayer MoS₂, neglecting the effects of spin-orbit coupling, which are not directly relevant for the mechanisms discussed here. Using the highest valence band and the lowest two conduction bands, we then construct an effective Wannier-Hamiltonian from projections onto the three dominant d -orbitals $\alpha, \beta \in \{d_{z^2}, d_{xy}, d_{x^2-y^2}\}$ of the Mo-atoms.

The resulting Fermi surfaces and the corresponding segments of the band structure are shown in Fig. 1(a) for two different electron doping levels. There are two prominent minima in the lowest conduction band [28]. The lower-energy minimum is at the K-points, whereas the higher-energy minimum is at $\Sigma = \frac{1}{2}|\Gamma K|$. Hence, this two-valley band structure of MoS₂ represents a situation where the Fermi surface topology changes with electron doping. At sufficiently low doping ($x \lesssim 0.06$, x in electrons per unit cell), the Fermi pockets are all centered around the K-points in the Brillouin zone corners (blue lines in right panel of Fig. 1(a)), whereas for $x \gtrsim 0.06$ the conduction band minima at Σ are also populated by electrons (red lines in right panel of Fig. 1(a)). As we show below, such a Lifshitz transition has a profound influence on the competition between Coulomb repulsion and electron-phonon coupling.

In the following we specifically examine the influence of screened Coulomb interactions on superconducting pairing, which depends on the electron doping level and on the dielectric environment. The available *screening channels* can be divided into *internal* and *external* channels, which independently contribute to the strength of the renormalized Coulomb interactions. Here, internal processes refer to the screening due to transitions between electronic states within the MoS₂ layer. The external screening arises due to the polarizability of adjacent substrates or adsorbates with dielectric constant ϵ_{sub} . We obtain the resulting renormalized Coulomb coupling constants in the following way (see supplemental material for more details). First, we derive realistic screened orbital dependent interaction matrix elements for the free-standing undoped material via RPA-calculations using the Spex and FLEUR software codes [29, 30]. The bare $U_{\alpha\beta}(q)$ and intrinsically screened (undoped material with *inter-band* transitions only) matrix elements $V_{\alpha\beta}(q)$ are then parametrized as functions of momentum transfer q . Next, the *external* screening effects of the dielectric background are accounted for by solving the Poisson equation for a continuous medium representing the dielectric environment. Specifically, we consider the geometric substrate-monolayer-substrate arrangement shown in the inset of Fig. 1(b). This allows us to compute the renormalized matrix elements $V_{\alpha\beta}(q)$ using the recently developed Wannier function continuum electrostatics approach [31]. To this end, we need to assign a physical thickness $d = 7.6 \text{ \AA}$ to the monolayer of MoS₂, approximately corresponding to the separation of adjacent layers in the bulk phase.

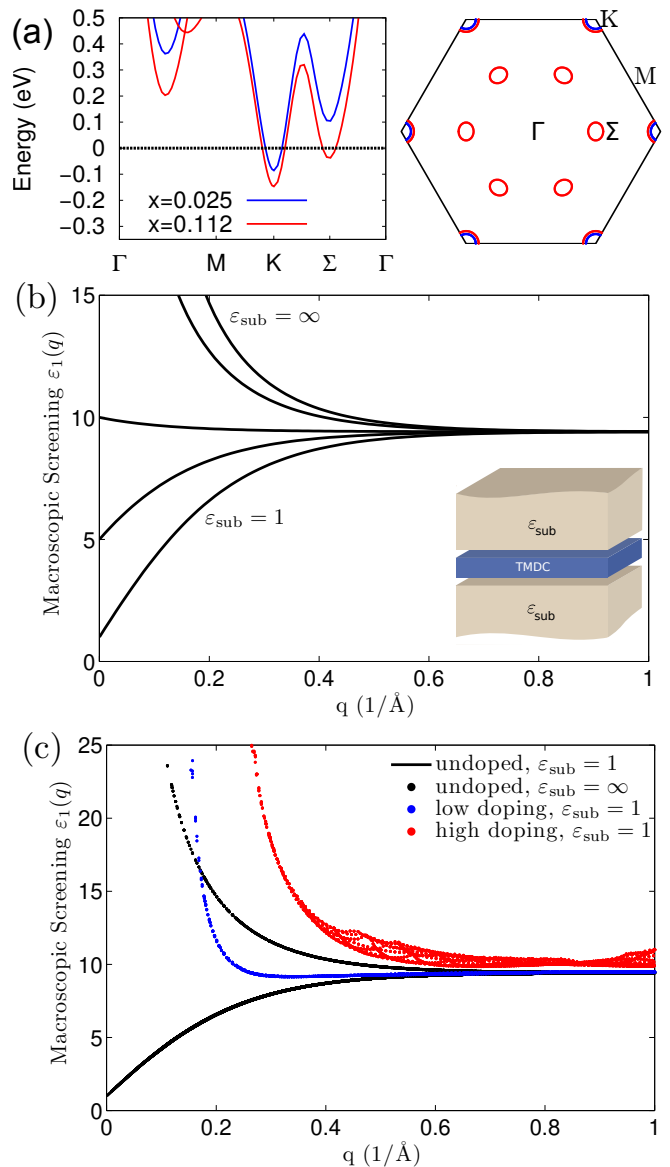


FIG. 1: (Color online) **(a)** Band structures and Fermi surfaces of MoS₂ at doping levels $x = 0.025$ and 0.112 electrons per unit cell; the black line is the Fermi energy. **(b)** Macroscopic screening $\epsilon_1(q)$ from fit model; the substrate dielectric constants used for $\epsilon_1(q)$ are $\epsilon_{\text{sub}} = 1, 5, 10, 50, \infty$. **(c)** Full screening for the undoped system with different surroundings as well as for low and high doping with vacuum surrounding.

The dielectric function $\epsilon_1(q)$ resulting from inter-band and background screening is shown in Fig. 1(b) for different dielectric environments of the MoS₂ monolayer [40]. In the long-wavelength limit, $\epsilon_1(q)$ is fully determined by the dielectric background: $\epsilon_1(q \rightarrow 0) = \epsilon_{\text{sub}}$. In the opposite limit ($q \gtrsim 1 \text{ \AA}^{-1}$), screening in the undoped case is solely due to the microscopic inter-band polarizability of the MoS₂ layer itself, $\epsilon_1(q) \approx 9.4 \equiv \epsilon_{\infty}$, but unaffected by the dielectric environment [31, 32].

In addition to the background and inter-band screen-

ing, we also have to include metallic intra-band screening by the conduction electrons in the case of electron doping. We then arrive at the fully screened static Coulomb interaction $\hat{W}(q) = \hat{V}(q) \cdot (1 - \hat{V}(q)\hat{\Pi}_0(q))^{-1}$, where $\hat{\Pi}_0(q)$ is the intra-band polarizability and where $\hat{W}(q)$, $\hat{V}(q)$ and $\hat{\Pi}_0(q)$ are matrices in the Wannier function basis. The polarizability is obtained using RPA for the lowest conduction band [33]. In Fig. 1(c) we compare dielectric functions including only inter-band and background screening (for $\varepsilon_{\text{sub}} = 1$ and $\varepsilon_{\text{sub}} = \infty$) with dielectric functions including all screening channels, i.e. the combined effect of external background (for $\varepsilon_{\text{sub}} = 1$) and all internal screening processes. In all metallic scenarios, either due to a metallic environment ($\varepsilon_{\text{sub}} = \infty$) or sufficient electron doping of the MoS₂ monolayer, we find a divergent $\varepsilon \sim 1/q$ for small momenta q . Furthermore, in the doping induced metallic regime we observe strong dependencies on the doping level.

Effects of internal and external screening on Coulomb interactions. Using the fully screened interaction matrix elements $\hat{W}(q)$, we can compute the intra- and inter-valley Coulomb coupling constants [21]

$$\mu_\gamma = \frac{1}{N(E_F)} \sum_{\mathbf{k}\mathbf{k}'}^\gamma W_{\mathbf{k}\mathbf{k}'} \delta(\epsilon_{\mathbf{k}} - E_F) \delta(\epsilon_{\mathbf{k}'} - E_F), \quad (1)$$

which are Fermi surface averages of the screened Coulomb interaction, including scattering processes with initial states $\{\mathbf{k}, \mathbf{k}'\}$ and final states $\{\mathbf{k}', \mathbf{k}\}$ (i.e. $\mathbf{q} = \mathbf{k} - \mathbf{k}'$). Here the momenta \mathbf{k} and \mathbf{k}' are on the same (different) Fermi surface segments for $\gamma = \text{intra}$ ($\gamma = \text{inter}$). In Eq. (1) $\hat{W}(q) \rightarrow W_{\mathbf{k}\mathbf{k}'} = \langle (\mathbf{k}', -\mathbf{k}') | \hat{W}(k - k') | (\mathbf{k}, -\mathbf{k}) \rangle$ has been transformed from the orbital basis to the band basis, and we only consider the lowest conduction band for $W(q)$ since it is the only band that crosses the Fermi level for the electron doping concentrations considered here.

The resulting effective Coulomb coupling constants $\mu = \sum_\gamma \mu_\gamma$ are shown in Fig. 2(a) for different dielectric environments of the MoS₂ layer and in dependence of the electron doping concentration. In the low-doping regime, $x \lesssim 0.06$, where only the Fermi pockets around K and K' are present, the coupling μ is renormalized by up to $\sim 30\%$ via external screening. In contrast, at higher doping concentrations μ is clearly much less sensitive to its dielectric environment, and variations of μ due to external screening are limited to $\sim 10\%$. A comparison of external screening effects on intra- and inter-valley Coulomb scattering (Fig. 2(b)) shows that essentially only the intra-valley scattering is affected by substrates, capping layers etc. These two observations can be explained intuitively. External screening is most effective when the separation ($\sim 1/q$) of the interacting charges inside the monolayer is *larger* than the distance $\sim \frac{1}{2}d$ to their image charges in the environment but *smaller* than the internal Thomas Fermi screening length $1/q_{\text{TF}}$, i.e. for $q_{\text{TF}} < q < \frac{2}{d}$ (cf.

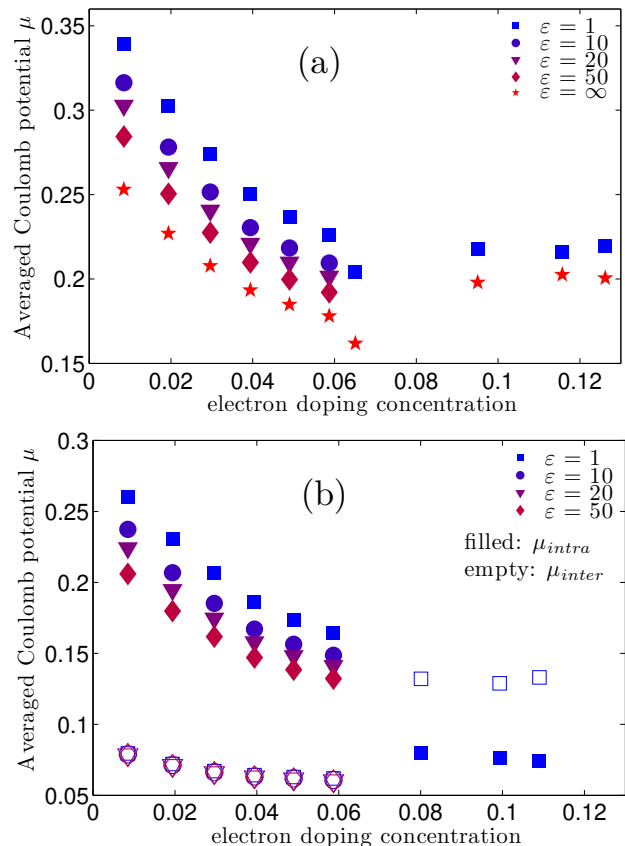


FIG. 2: (Color online) Dependence of Coulomb coupling constants on the electron doping concentration x , subject to various ε_{sub} of the dielectric environment. In (a) the full coupling constant μ is shown. In (b) we present the partial *inter-valley* μ_{inter} (empty symbols) and *intra-valley* μ_{intra} (filled symbols).

Fig. 1(c)). As a consequence, the influence of the substrate weakens as soon as $q_{\text{TF}} \gtrsim \frac{2}{d}$. Using a typical TMDC monolayer thickness of $d \approx 7.6 \text{ \AA}$, a Thomas-Fermi wave vector $q_{\text{TF}} = 2\pi e^2 N(E_F) / (A \varepsilon_1(q_{\text{TF}}))$, and a background dielectric constant of the TMDCs on the order of $\varepsilon_1(q) \approx \varepsilon_\infty = 9.4$ for $q > \frac{2}{d}$, we find that the substrate influence is minor as soon as the density of states at the Fermi level exceeds $N(E_F) \gg 0.23 / \text{eV}$ per unit cell.

In MoS₂, we have $N(E_F) \approx 0.4 \text{ eV}^{-1}$ and $N(E_F) \approx 2 \text{ eV}^{-1}$ for low ($x < 0.06$) and high electron doping concentrations ($x > 0.06$), respectively, which means that substrate influence is weak, especially in the regime of high doping concentrations. However, for sufficiently low doping concentrations, the scattering inside the same K- or K'-valley can be controlled via the substrates.

Coulomb driven superconductivity. In general, superconductivity occurs when the total coupling between electrons is attractive, $\mu_{\text{tot}} < 0$, i.e. when either the effective coupling between electrons mediated by phonons overcomes the electron-electron repulsion or

when the inter-valley coupling of the electrons is larger than the intra-valley coupling [21]. If there are only two Fermi pockets around K and K', which is the case for monolayer MoS₂ in the low electron doping regime ($x \lesssim 0.06$), purely electronically mediated superconductivity with an unconventional sign changing order parameter ($\Delta_K = -\Delta_{K'}$) could in principle occur for sufficiently low temperatures if $\mu_{\text{inter}} > \mu_{\text{intra}}$. However, as one can see from Fig. 2(b), this situation is neither realized in freestanding MoS₂ nor can it be achieved using substrates or capping layers with arbitrarily large (q independent) dielectric constants. I.e. for unconventional electron driven superconductivity in MoS₂ one would need more complex mechanisms involving a stronger renormalization of the interactions at low energies than what can be achieved via substrates [22].

Electron phonon coupling driven superconductivity: In the framework of Eliashberg theory [34], the Allen-Dynes formula [35] yields an estimate of the critical temperature,

$$T_c = \frac{\hbar\omega_{\text{log}}}{1.2k_B} \exp \left[\frac{-1.04(1 + \lambda)}{\lambda(1 - 0.62\mu^*) - \mu^*} \right], \quad (2)$$

which accounts for the competition of the phonon driven attractive interaction entering via the effective coupling strength λ and the typical phonon frequency ω_{log} with the Coulomb interaction expressed by the Morel-Anderson parameter μ^* [36]. The phononic parameters for MoS₂ have been calculated in Refs. [24, 25]. The coefficient μ^* that describes the Coulomb repulsion is obtained using the formula given by Morel and Anderson [36] for the retarded Coulomb potential,

$$\mu^* = \frac{\mu}{1 + \mu \ln \left[\frac{E_F}{\omega_{\text{log}}} \right]}. \quad (3)$$

In Fig. 3, we plot the dependence of μ^* on the electron doping level for freestanding MoS₂ and MoS₂ embedded in a perfect metallic environment. For free-standing MoS₂ we observe a decrease of μ^* from $\mu^* \approx 0.3$ to $\mu^* \lesssim 0.2$ for $x \lesssim 0.06$, which is caused by the corresponding decrease in μ . At larger electron doping concentrations, μ is basically constant, and we observe a slight decrease to $\mu^* \lesssim 0.15$ because of the decrease in the phonon frequency ω_{log} (see Ref. [25]). For MoS₂ embedded in a metallic environment, μ^* shows essentially the same trend with the only difference in comparison to the free-standing case being a slight reduction of μ^* , particularly at low doping.

A significant T_c is only reached when the exponent in Eq. (2) is close to -1 or larger, especially when the electrons mainly couple to acoustic phonons and thus ω_{log} is rather small, e.g. $T_c \gtrsim \frac{\hbar\omega_{\text{log}}}{1.2k_B} e^{-2}$. To achieve this, $\lambda > 3\mu^*$ has to be realized given the range of $0.1 < \mu^* < 0.35$ found here. From the comparison of μ^* and $\lambda/3$ in Fig. 3, we see that a significant T_c (as occurring for $\lambda > 3\mu^*$)

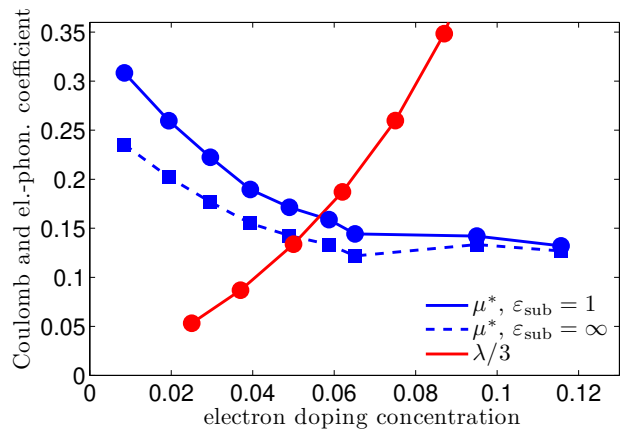


FIG. 3: (Color online) Retarded Coulomb potential μ^* used in Eliashberg theory and effective electron-phonon coupling strength λ in dependence of the electron doping concentration x . μ^* for the freestanding monolayer ($\epsilon_{\text{sub}} = 1$) and in the presence of a metallic environment ($\epsilon_{\text{sub}} = \infty$). λ is scaled by a factor of $1/3$.

can only be observed when both valleys in the conduction band are occupied by electrons, i.e., once $x \gtrsim 0.06$.

We thus conclude that the frequent use of a constant for the Coulomb pseudopotential, e.g. $\mu^* = 0.13$ [24, 31, 37], is not sufficient in the case of electron doped MoS₂ to describe the influence of the Coulomb interaction directly at the transition to the superconducting phase. However, the drop in the critical temperature of TMDCs [6, 7, 9, 16, 18] when going from the bulk or multilayer-system to a monolayer cannot be caused by enhanced Coulomb interactions, because the values of the electron-phonon coupling are much larger than the $\mu^* \approx 0.15$, which we find in the region of optimal doping independently of the dielectric environment of the MoS₂ monolayer.

Conclusions: The microscopic description of the Coulomb interactions in the electron doped monolayer MoS₂ developed here reveals a clear decrease of the retarded Coulomb potential with increasing doping, which renders the frequent use of constant doping and material independent μ^* questionable. Comparing the values for the electron-phonon interaction in Ref. [25] with the retarded Coulomb potential μ^* and the valley decomposed electron-electron interaction coupling constants presented here, we conclude that the superconductivity in MoS₂ is electron-phonon driven and has an onset at electron doping levels when both valleys in the conduction band are occupied. The effects of substrates turn out to be relatively small, at least around optimal doping, and we find that the experimentally observed reduction of the critical temperature upon approaching the monolayer limit [18] is not caused by enhanced Coulomb interactions, i.e. lack of screening as the dimensionality of the material is reduced. This conclusion should be generally applicable also to other superconducting 2d

materials such as NbSe₂ [9] and particularly the electron doped TMDCs like WS₂ or MoSe₂ [10, 11] because of their similar electronic and phononic structure.

Acknowledgments: S.H. would like to thank the Humboldt Foundation for support. This work was supported by the European Graphene Flagship and by the Department of Energy under Grant No. DE-FG02-05ER46240. The numerical computations were carried out on the Norddeutscher Verbund zur Förderung des Hoch- und Höchstleistungsrechnens (HLRN) cluster.

-
- [1] R. B. Somoano, V. Hadek, A. Rembaum, S. Samson, and J. A. Woollam, *The Journal of Chemical Physics* **62**, 1068 (1975).
- [2] J. A. Woollam and R. B. Somoano, *Materials Science and Engineering* **31**, 289 (1977).
- [3] J. Paglione and R. L. Greene, *Nat Phys* **6**, 645 (2010).
- [4] K. Taniguchi, A. Matsumoto, H. Shimotani, and H. Takagi, *Appl. Phys. Lett.* **101**, 042603 (2012).
- [5] J. T. Ye *et al.*, *Science* **338**, 1193 (2012).
- [6] X. Xi *et al.*, *Nat. Nano.* **10**, 765 (2015).
- [7] Y. Yu *et al.*, *Nat. Nano.* **10**, 270 (2015).
- [8] J. K. Glasbrenner *et al.*, *Nat Phys* **11**, 953 (2015).
- [9] Y. Cao *et al.*, *Nano Lett.* **15**, 4914 (2015).
- [10] S. Jo, D. Costanzo, H. Berger, and A. F. Morpurgo, *Nano Lett.* **15**, 1197 (2015).
- [11] W. Shi *et al.*, *Sci. Rep.* **5** (2015).
- [12] W. Qing-Yan *et al.*, *Chinese Physics Letters* **29**, 037402 (2012).
- [13] S. Coh, M. L. Cohen, and S. G. Louie, *New Journal of Physics* **17**, 073027 (2015).
- [14] J.-F. Ge *et al.*, *Nat Mater* **14**, 285 (2015).
- [15] C. Tang *et al.*, *Phys. Rev. B* **93**, 020507 (2016).
- [16] R. Frindt, *Phys. Rev. Lett.* **28**, 299 (1972).
- [17] J. Biscaras, Z. Chen, A. Paradisi, and A. Shukla, *Nat Commun* **6**, 8826 (2015).
- [18] D. Costanzo, S. Jo, H. Berger, and A. F. Morpurgo, *Nat Nano* **11**, 339 (2016).
- [19] J. M. Lu *et al.*, *Science* **350**, 1353 (2015).
- [20] Y. Saito *et al.*, *Nat Phys* **12**, 144 (2016).
- [21] R. Roldan, E. Cappelluti, and F. Guinea, *Phys. Rev. B* **88**, 054515 (2013).
- [22] J. Yuan and C. Honerkamp, arXiv:1504.04536 [cond-mat] (2015), arXiv: 1504.04536.
- [23] N. F. Q. Yuan, K. F. Mak, and K. T. Law, *Phys. Rev. Lett* **113**, 097001 (2014).
- [24] Y. Ge and A. Y. Liu, *Phys. Rev. B* **87**, 241408 (2013).
- [25] M. Rösner, S. Haas, and T. O. Wehling, *Phys. Rev. B* **90**, 245105 (2014).
- [26] T. Das and K. Dolui, *Phys. Rev. B* **91**, 094510 (2015).
- [27] P. Giannozzi *et al.*, *J. Phys.: Condens. Matter* **21**, 395502 (2009).
- [28] A. Kuc, N. Zibouche, and T. Heine, *Phys. Rev. B* **83**, 245213 (2011).
- [29] C. Friedrich, S. Blügel, and A. Schindlmayr, *Phys. Rev. B* **81**, 125102 (2010).
- [30] The juelich fleur project, <http://www.flapw.de/pm/index.php>.
- [31] M. Rösner, E. Sasioglu, C. Friedrich, S. Blügel, and T. O. Wehling, *Phys. Rev. B* **92**, 085102 (2015).
- [32] K. Andersen, S. Latini, and K. S. Thygesen, *Nano Lett.* **15**, 4616 (2015).
- [33] R. E. Groenewald, M. Rösner, G. Schönhoff, S. Haas, and T. O. Wehling, arXiv:1601.01707 [cond-mat] (2016), arXiv: 1601.01707.
- [34] G. M. Eliashberg, *Sov. Phys. JETP* **11**, 696 (1960).
- [35] P. B. Allen and R. C. Dynes, *Phys. Rev. B* **12**, 905 (1975).
- [36] P. Morel and P. W. Anderson, *Phys. Rev.* **125**, 1263 (1962).
- [37] W. L. McMillan, *Phys. Rev.* **167**, 331 (1968).
- [38] A. Steinhoff, M. Rösner, F. Jahnke, T. O. Wehling, and C. Gies, *Nano Lett.* **14**, 3743 (2014).
- [39] The electron doping level is given as the number of additional electrons per unit cell of molybdenum disulfide.
- [40] The function $\varepsilon_1(q)$ describes macroscopic screening effects. The functions $\varepsilon_{2,3}$, describing only microscopic screening, are discussed in the supplement.

SUPPLEMENTAL MATERIAL TO "INTERPLAY OF SCREENING AND SUPERCONDUCTIVITY IN LOW-DIMENSIONAL MATERIALS"

PARAMETRIZATION OF BACKGROUND AND SUBSTRATE SCREENING

Our calculations and the parametrization of the Coulomb interaction were previously described in [38]. Here, we follow a similar procedure and make use of the Wannier function continuum electrostatics approach [31] to include the screening effects of substrates, as described in the following.

The bare interaction matrix $U_{\alpha\beta}(q)$ in the orbital basis $\alpha, \beta \in \{d_{z^2}, d_{xy}, d_{x^2y^2}\}$ is obtained for the freestanding undoped material via RPA-calculations using the Spex and FLEUR software code [29, 30]. To parametrize the matrix elements, we use the formula

$$U_{\alpha\beta}(q) = \frac{e^2}{2\varepsilon_0 A} \frac{1}{q(1 + \gamma_{\alpha\beta}q)} \quad (4)$$

with the area of the 2D hexagonal unit cell $A = \frac{\sqrt{3}}{2}a^2$ and the lattice parameter $a = 3.18 \text{ \AA}$. $\gamma_{\alpha\beta}$ describes how the effective height affects short wavelengths, which means that it is a structure factor which plays the role of an orbital specific effective height of the film and becomes important at large wavevectors q . The values of $\gamma_{\alpha\beta}$ are shown in Tab. I.

TABLE I: Parameters for the effective height $\gamma_{\alpha\beta}$ of MoS_2 , taken from [38].

| orbitals | | γ (Å) |
|--------------|--------------|--------------|
| d_{z^2} | d_{z^2} | 1.99 |
| d_{z^2} | d_{xy} | 2.42 |
| d_{z^2} | $d_{x^2y^2}$ | 2.40 |
| d_{xy} | d_{xy} | 2.32 |
| d_{xy} | $d_{x^2y^2}$ | 2.46 |
| $d_{x^2y^2}$ | $d_{x^2y^2}$ | 2.27 |

To calculate the background screened Coulomb interaction, we use the sorted eigenbasis of the bare interaction

$$U^{\text{diag}}(q) = \begin{pmatrix} U_1^{\text{diag}}(q) & 0 & 0 \\ 0 & U_2^{\text{diag}}(q) & 0 \\ 0 & 0 & U_3^{\text{diag}}(q) \end{pmatrix} \quad (5)$$

where $U_1^{\text{diag}}(q)$ is the leading eigenvalue. The screened matrix elements are then given by an elementwise calculation using the background screening $\varepsilon(q)$,

$$V_i^{\text{diag}}(q) = \varepsilon_i^{\text{diag}}(q)^{-1} U_i^{\text{diag}}(q) \quad (6)$$

which we transform back to the orbital basis using the

eigenvectors of $U_{\alpha\beta}(q)$. The formula for the screening is

$$\varepsilon^{\text{diag}}(q) = \begin{pmatrix} \varepsilon_1(q) & 0 & 0 \\ 0 & \varepsilon_2 & 0 \\ 0 & 0 & \varepsilon_3 \end{pmatrix} \quad (7)$$

where the constants $\varepsilon_2 = 3.035$ and $\varepsilon_3 = 2.448$ describe microscopic screening effects which are similar to the bulk. The macroscopic effects are described via

$$\beta_i = \frac{\varepsilon_\infty - \varepsilon_{\text{sub},i}}{\varepsilon_\infty + \varepsilon_{\text{sub},i}}$$

$$\varepsilon_1(q) = \varepsilon_\infty \frac{1 - \beta_1\beta_2 e^{-2qd}}{1 + (\beta_1 + \beta_2)e^{-qd} + \beta_1\beta_2 e^{-2qd}}. \quad (8)$$

where the parameters are derived from ab initio calculations yielding $d = 7.605 \text{ \AA}$, $\varepsilon_\infty = 9.411$, and the surrounding substrates have dielectric constants $\varepsilon_{\text{sub},1}$ above and $\varepsilon_{\text{sub},2}$ below the monolayer. In the case of vacuum surrounding the monolayer, $\varepsilon_{\text{sub},1} = \varepsilon_{\text{sub},2} = 1$, eq. 8 simplifies to

$$\varepsilon_1(q) = \varepsilon_\infty \frac{\varepsilon_\infty + 1 - (\varepsilon_\infty - 1)e^{-qd}}{\varepsilon_\infty + 1 + (\varepsilon_\infty - 1)e^{-qd}}. \quad (9)$$

The macroscopic screening for various substrates and the microscopic screening are shown in Fig. 4.

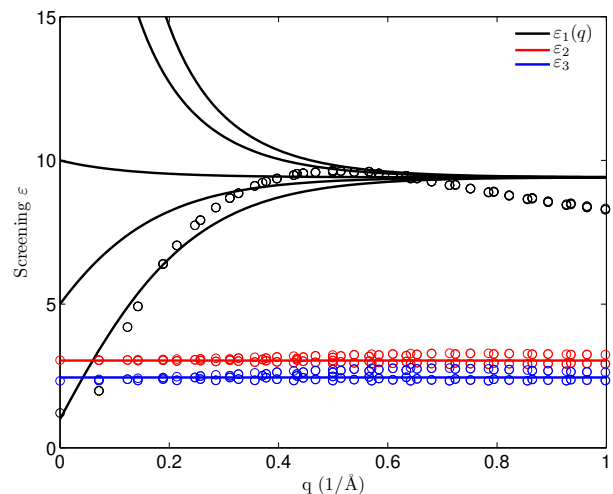


FIG. 4: Macroscopic screening $\varepsilon_1(q)$ and microscopic screenings $\varepsilon_2, \varepsilon_3$. From bottom to top, the substrate dielectric constants used for $\varepsilon_1(q)$ are $\varepsilon_{\text{sub}} = 1, 5, 10, 50, \infty$. The empty circles show the ab initio data for the screening without substrates.

REALISTIC COULOMB MATRIX ELEMENTS

The bare and screened Coulomb matrix elements are given in Tab. II.

TABLE II: Bare onsite U as well as background screened onsite V and fully screened onsite Coulomb matrix elements W for the three important orbitals in real space. Values for W are in the range of low electron doping $x \approx 0.04$ [39] in the fifth (W_{low} , K is occupied) and for high electron doping $x \approx 0.16$ in the last column (W_{high} , K and Σ are occupied).

| orbitals | | undoped | | doped | |
|---------------|---------------|----------|----------|-----------------------|------------------------|
| | | U (eV) | V (eV) | W_{low} (eV) | W_{high} (eV) |
| d_{z^2} | d_{z^2} | 8.90 | 2.00 | 0.98 | 0.71 |
| d_{z^2} | d_{xy} | 8.17 | 1.76 | 0.79 | 0.51 |
| d_{z^2} | $d_{x^2-y^2}$ | 8.20 | 1.77 | 0.79 | 0.51 |
| d_{xy} | d_{xy} | 8.33 | 1.89 | 0.96 | 0.65 |
| d_{xy} | $d_{x^2-y^2}$ | 8.11 | 1.77 | 0.83 | 0.53 |
| $d_{x^2-y^2}$ | $d_{x^2-y^2}$ | 8.41 | 1.91 | 0.97 | 0.66 |